Research article

JGS
Journal of the Geological Society

https://doi.org/10.1144/jgs2025-040 | Vol. 183 | 2025 | jgs2025-040

Persistent oxygenation of the Mesoproterozoic shallow ocean: evidence from the *c.* 1.44-billion-year-old Tieling Formation, North China Craton

Kun Zhang[1]*, Lanyun Miao[2], Shihong Zhang[3], Ying Zhou[1] and Graham Shields[1]

[1] Department of Earth Sciences, University College London, London WC1E 6BT, UK
[2] State Key Laboratory of Palaeobiology and Stratigraphy, Nanjing Institute of Geology and Palaeontology, Chinese Academy of Sciences, Nanjing 210008, China
[3] State Key Laboratory of Biogeology and Environmental Geology, China University of Geosciences, Beijing 100083, China
KZ, 0000-0002-4346-9525; LM, 0000-0003-3354-2319
* Correspondence: kun-zhang@ucl.ac.uk

Abstract: The Mesoproterozoic era experienced dynamic variability in atmosphere–ocean oxygen levels. Recent studies suggest that a pulse of oxygenation is recorded in the *c.* 1.44 Ga Tieling Formation but the duration of this event remains unclear. Here, we report relatively high-resolution carbonate carbon isotope ($\delta^{13}C$), rare earth element (REE) and I/(Ca + Mg) data from the Tieling Formation at Jixian, North China. The $\delta^{13}C$ values reveal a limited range, mainly between −2 and +1‰, and systematic stratigraphic trends. The lower member of the formation is characterized by manganiferous carbonates with light and middle REE-enriched patterns and relatively high but scattered I/(Ca + Mg) values. We interpret these geochemical signals in terms of the early diagenetic reduction of primary Mn oxides. The upper member, by contrast, exhibits stratigraphic covariation between negative Ce anomalies and I/(Ca + Mg) ratios that we attribute to sea-level change rather than oxygenation. The geochemical data from both lower and upper members support vigorous oxidative Mn cycling, thus suggesting that an oxygenated shallow ocean probably persisted for millions of years in the Mesoproterozoic.

Keywords: Mesoproterozoic; Shallow seawater redox; Oxygenation; I/(Ca + Mg); REE

Supplementary material: Supplementary figures and data are available at https://doi.org/10.6084/m9.figshare.c.7941409

Thematic collection: This article is part of The North China Craton as a window to Earth's middle age collection available at: https://www.lyellcollection.org/topic/collections/the-north-china-craton-as-a-window-to-earths-middle-age

Received 29 January 2025; **revised** 11 June 2025; **accepted** 3 July 2025

The oxygenation of Earth's surface environment has now generally been constructed as a non-linear process with stepwise increases in oxygen during the Great Oxidation Event, Neoproterozoic Oxygenation Event and Paleozoic Oxygenation Event (Bekker *et al.* 2004; Canfield 2005; Dahl *et al.* 2010; Och and Shields-Zhou 2012; Lyons *et al.* 2014; Krause *et al.* 2018). The mid-Proterozoic (*c.* 1.8–0.8 Ga), sandwiched between the two Proterozoic oxygenation events, was previously considered to have been an interval of relative stasis in terms of environmental evolution (Buick *et al.* 1995; Brasier and Lindsay 1998). However, emerging geochemical and palaeontological evidence demonstrates that there were probably significant spatiotemporal variabilities in atmosphere–ocean redox conditions (Lyons *et al.* 2021), as well as underestimated eukaryotic multicellularity (Zhu *et al.* 2016; Miao *et al.* 2024).

Marine oxygenation events have been documented from the *c.* 1.56 Ga Gaoyuzhuang Formation (Zhang *et al.* 2018; Shang *et al.* 2019; Luo *et al.* 2021), the *c.* 1.4 Ga Xiamaling Formation (Zhang *et al.* 2016), Kaltasy Formation (Sperling *et al.* 2014) and Velkerri Formation (Mukherjee and Large 2016; Yang *et al.* 2017), and the *c.* 1.3–1.0 Ga Shennongjia Group (Canfield *et al.* 2018; Meng *et al.* 2025; Wei *et al.* 2025). More recently, the *c.* 1.44 Ga Mesoproterozoic Tieling Formation that unconformably underlies the Xiamaling Formation has received increasing attention. This is because its existing geochemical data such as carbonate I/(Ca + Mg), Cr isotopes and Ce anomalies imply a transient increase in oxygen levels (Hardisty *et al.* 2017; Wei *et al.* 2021; Yu *et al.* 2022, 2025). However, the duration and extent of this potential oxygenation event remain contentious. Moreover, the recent study suggests that the Wafangzi Mn deposit in the lower member of the Tieling Formation provides evidence for oxygenated seawater (Yan *et al.* 2024). The Mesoproterozoic is traditionally viewed as an interval of 'Mn hiatus' (Roy 2006; Maynard 2010; Robbins *et al.* 2023). Hence, the occurrence of Mn deposits in the Tieling Formation with the contemporaneous *c.* 1.45 Ga Mn deposits in the Ullawarra Formation in Australia (Spinks *et al.* 2023) might suggest oxygenation on a broader scale. However, there is so far little convincing evidence from the lower member carbonates of the Tieling Formation at other localities. In this study, we present a relatively high-resolution multiproxy geochemical dataset including carbonate carbon isotope ($\delta^{13}C$), Ce anomaly and I/(Ca + Mg) data for the Tieling Formation at Jixian, North China. These results, together with published data, provide evidence for a locally to regionally sustained oxygenated shallow ocean for millions of years in the Mesoproterozoic.

Geological setting

The North China Craton was in a long-term extensional tectonic setting through late Paleoproterozoic to Neoproterozoic time, during which four major sedimentary basins, including the Xiong'er rift, the Yanliao rift, the Zhaertai–Bayan Obo rift and the eastern marginal rift, developed above the Archean to early Paleoproterozoic basement (Lu *et al.* 2008; Zhai *et al.* 2015). The Yanliao Basin is located on the central to northern margin of the

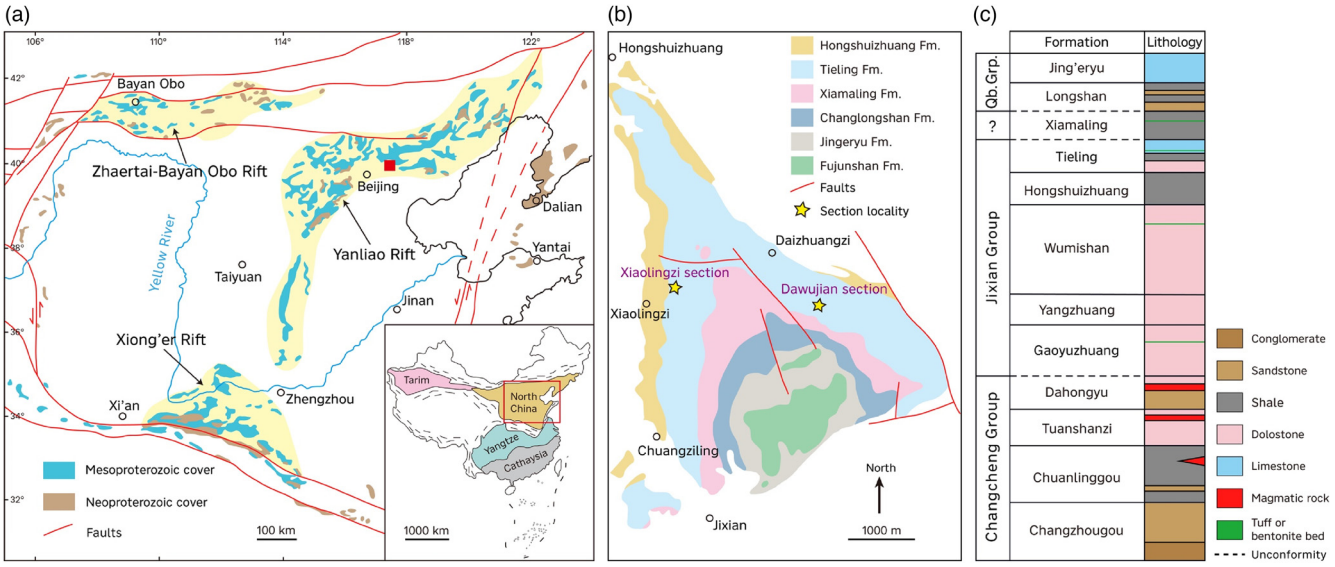

Fig. 1. (**a**) Geological map showing the Mesoproterozoic and Neoproterozoic outcrops on the North China Craton. The red square indicates the location of Jixian, Tianjin Municipality. The inset map shows the present location of the North China Craton. (**b**) Simplified geological map of the study area. The studied sections are denoted by yellow stars. (**c**) Simplified stratigraphical column of the Proterozoic strata in the Yanliao Basin, North China. Qb., Qingbaikou. Source: (a) modified after Hu *et al.* (2016); (b) modified after Tang *et al.* (2017) and Yu *et al.* (2022); (c) modified after Miao *et al.* (2021).

North China Craton (Fig. 1). It contains a thick sedimentary sequence that is traditionally divided into four groups, in ascending order, namely the Changcheng Group, Jixian Group, Xiamaling Formation and Qingbaikou Group (Hu *et al.* 2016; Fig. 1).

The Tieling Formation, the focus of this study, is the uppermost unit of the Jixian Group. At Jixian, the Tieling Formation is about 330 m thick and is subdivided into lower (Daizhuangzi) and upper (Laohuding) members. The lower member conformably overlies the Hongshuizhuang Formation and comprises thick sandstone at its base. Upsection, the lithology is dominated by manganiferous dolostone with intercalated shale, which transitions into predominantly greenish shale near its top (Fig. 2). The unconformably overlying upper member is mainly composed of limestone and dolomitic limestone. It is characterized by thick stromatolitic limestone in the upper part in which the presence of glauconite has also been documented (Mei *et al.* 2008; Zhou *et al.* 2009; Tang *et al.* 2017; Fig. 2). Near its top, the upper member is dominated by an alternation of thin bands of limestone and mudstone that are unconformably overlain by the Xiamaling Formation (Fig. 2). It has been proposed that the lower member was mainly deposited in an intertidal setting, while the upper member was mainly deposited in subtidal and intertidal environments (Mei *et al.* 2008).

The bentonite layer near the bottom of the upper member of the Tieling Formation has been dated at 1437 ± 21 Ma (Su *et al.* 2010) and 1439 ± 14 Ma (Li *et al.* 2014) by SHRIMP zircon U–Pb analyses. More recently, laser ablation inductively coupled plasma mass spectrometry (LA-ICP-MS) zircon U–Pb ages of 1445 ± 12 and 1442 ± 10 Ma have also been obtained from the same bentonite layer at the Dawujian section, Jixian (Guo *et al.* 2019). The top of the Tieling Formation is considered to be younger than *c.* 1432 Ma based on cyclostratigraphic analysis of the carbonate rocks and older than *c.* 1418 Ma based on the zircon U–Pb age on bentonite from the bottom of the overlying Xiamaling Formation (Lyu *et al.* 2021). The age for the base of the Tieling Formation is relatively poorly constrained due to the absence of radiometric ages from both this interval and the underlying Hongshuizhuang Formation. Nevertheless, the next underlying Wumishan Formation has been dated at 1483 ± 13 and 1487 ± 16 Ma based on SHRIMP zircon U–Pb analyses on bentonite (Li *et al.* 2014), and hence, the base of the Tieling Formation is considered to be no older than 1.45 Ga (Tang *et al.* 2017).

Materials and methods

We collected 111 carbonate samples from the Tieling Formation along a road cut at the Dawujian section, and 11 carbonate samples from the lower member of the Tieling Formation at the Xiaolingzi section for comparison (Fig. 1). All samples were first broken into small fragments, and the fresh, vein-free part of the fragments was then microdrilled for geochemical analyses.

The carbonate content of each sample was estimated based on the weight of $CaCO_3$ and $MgCO_3$ assuming that Ca and Mg derived from nitric acid leaching were from the carbonate fraction. Based on the estimated carbonate content, approximately 200 μg of carbonate was weighed for C and O isotope analysis using a Thermo Delta V mass spectrometer coupled to a Gas Bench II device at the Bloomsbury Environmental Isotope Facility, University College London (UCL). Both $\delta^{13}C$ and $\delta^{18}O$ data are reported relative to Vienna Pee Dee Belemnite (VPDB). The external reproducibility of the NBS 19 standard was generally better than ±0.07‰ (1SD, $n = 8$) for both $\delta^{13}C$ and $\delta^{18}O$.

Rare earth elements (REE) were extracted using sequential leaching (Zhang and Shields 2023). In brief, approximately 50 mg of sample powder was pre-leached with 1 M pH-neutral ammonium acetate. The residues were rinsed with deionized water (18.2 MΩ), followed by partial leaching with 0.3 M acetic acid. After centrifugation, the supernatants were filtered into acid-cleaned Teflon beakers using 0.22 μm syringe filters, dried on a hot plate and redissolved in 2% HNO_3. The solutions were diluted in 2% HNO_3 and analysed for major and minor element concentrations on a Varian 720 inductively coupled plasma optical emission spectrometer (ICP-OES) at UCL. The leachates were then diluted to ~50 ppm Ca with 2% HNO_3 for trace element analysis (including REE) on an Agilent 7900 inductively coupled plasma mass spectrometer (ICP-MS) at UCL. The internal standard of 2 ppb indium was spiked to monitor instrumental drift and matrix effects. The formation of 2+ ions and oxide interference were monitored using Ba^{2+} and the formation rate of Ce oxide before analysis, respectively. Accuracy was monitored by two in-house bulk digested solution standards of SRM-88a and SGR-1, which generally gave the certified values within uncertainty. Repeated analysis of the drift monitor gave a relative standard deviation better than 5%. Blanks showed negligible concentrations below the

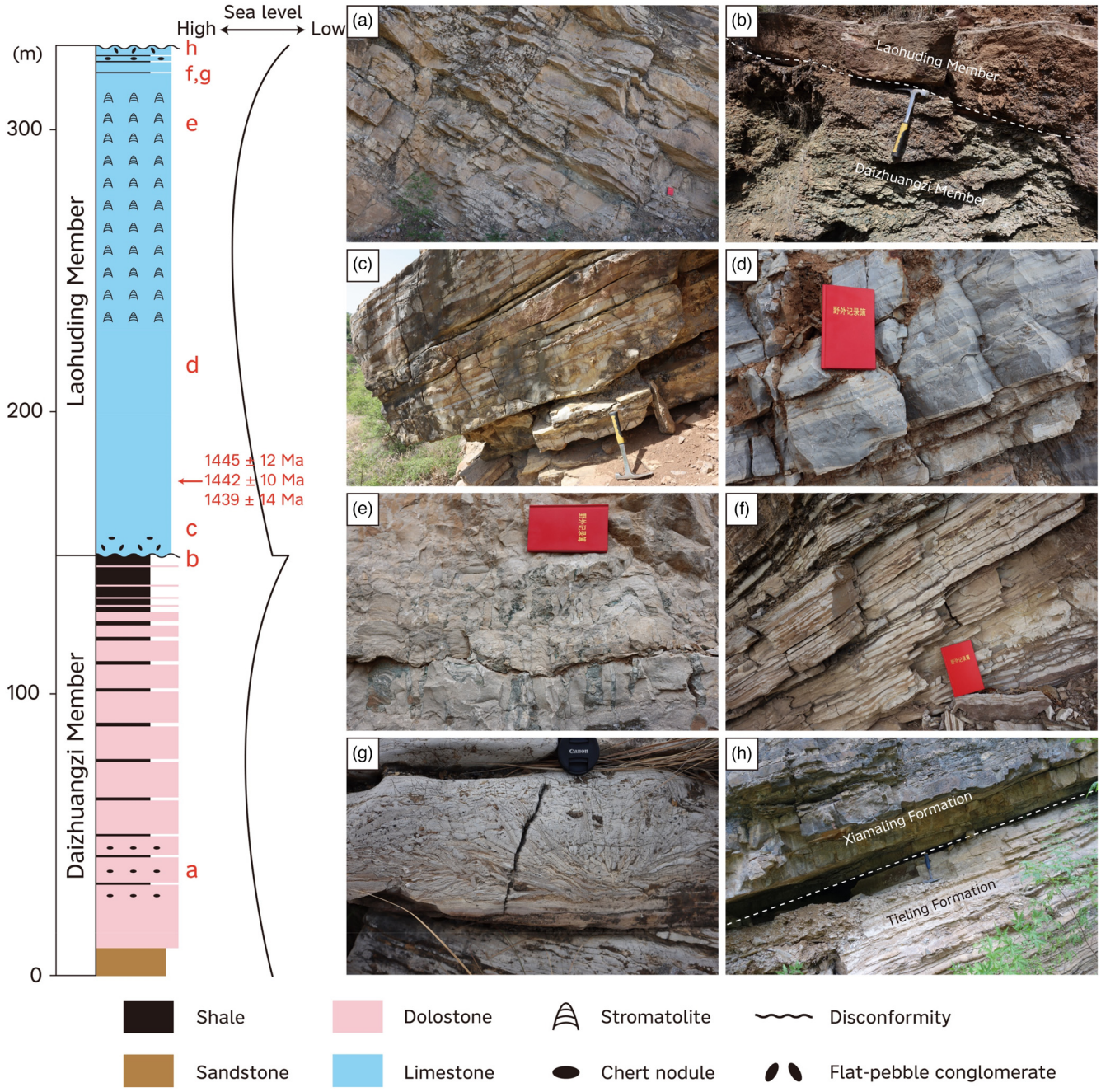

Fig. 2. General stratigraphic column and field photographs of the Tieling Formation at Jixian. Stratigraphic horizons of field photographs are marked on the stratigraphic column. (**a**) Bedded dolostone intercalated with shale; (**b**) disconformable contact between the Daizhuangzi and Laohuding members; (**c**) alternation of limestone and mudstone with limestone conglomerate; (**d**) bedded limestone; (**e**) stromatolite bearing glauconite; (**f**) alternation of limestone and mudstone bands; (**g**) flat-pebble conglomerate; (**h**) disconformable contact between the Tieling Formation and the Xiamaling Formation. Field photos in (a)–(c) were taken at Xiaolingzi while photos in (d)–(h) were taken at Dawujian. Source: the stratigraphic column is modified after Mei *et al.* (2008), Zhou *et al.* (2009) and Tang *et al.* (2016); the sea-level curve is from Mei *et al.* (2008); the age constraints are from Li *et al.* (2014) and Guo *et al.* (2019).

detection limit. REE concentrations are normalized against post-Archean Australian Shale (PAAS) values of Pourmand *et al.* (2012) (denoted by the subscript N). The Ce anomaly was calculated following Lawrence and Kamber (2006) as $Ce/Ce^* = Ce_N/(Pr_N^2/Nd_N)$.

The extraction and analysis of iodine in carbonate rocks largely followed the method of Zhang *et al.* (2024*a*). Briefly, ~5 mg of sample powder was cleaned with 1 ml deionized water, followed by leaching with 1 ml 3% HNO_3 in the ultrasonic bath for 10 min. After centrifugation the supernatant was transferred into the stabilizer (3% ethylenediaminetetraacetic acid in 3% ammonium hydroxide) for elemental analysis. Ca and Mg were analysed on a Varian 720 ICP-OES at UCL. Solution standards of SRM-88a and SGR-1 were analysed routinely to check the accuracy and gave the certified values. Iodine was analysed using an Agilent 7900 ICP-MS at UCL. Calibration standards were made freshly from potassium iodate powder, dissolved in the stabilizer with 100 ppm Ca matched to samples. Indium at 2 ppb was spiked beforehand as an internal standard to monitor instrumental drift and matrix effects. Analyses of JCp-1, CRM-393 and SRM-1c duplicates yielded I/Ca values of 4.24 ± 0.09 μmol/mol (1SD, $n = 4$), 0.45 ± 0.02 μmol/mol (1SD, $n = 4$) and 0.99 ± 0.08 μmol/mol (1SD, $n = 4$), respectively, which were comparable to published literature values (Lu *et al.* 2020; Zhang *et al.* 2024*a*).

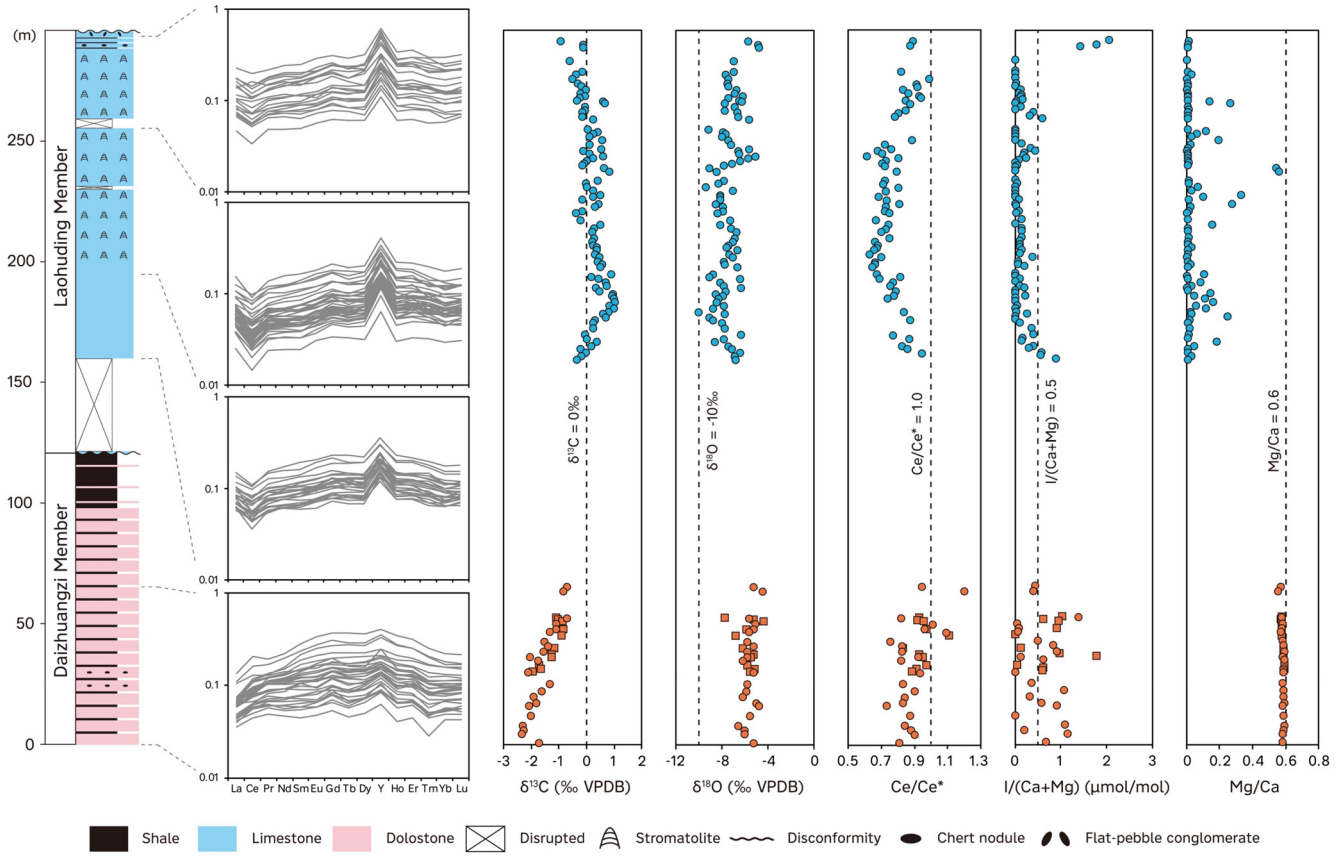

Fig. 3. Composite stratigraphic column and geochemical data for the Tieling Formation at the Dawujian section (circles). Geochemical data from the Xiaolingzi section (squares) are correlated based on $\delta^{13}C$ profiles. Note that iodine content below the detection limit is regarded as zero, and only filtered Ce/Ce* data are displayed.

Results and discussion

Formation of Mn-rich carbonates in the Daizhuangzi member of the Tieling Formation

The most striking feature of the lower member dolostone is the high Mn concentrations ranging between 1639 and 4677 ppm with a mean of 2543 ppm. Petrographic observation revealed a dominance of fine-grained carbonate crystals (Fig. S1), indicating that late diagenetic alteration is unlikely to explain the Mn enrichment. We suggest that the typical diagenetic model (Calvert and Pedersen 1996; Roy 2006), rather than the direct precipitation model (Herndon *et al.* 2018; Wittkop *et al.* 2020), is more in line with Mn enrichment in the Daizhuangzi carbonates. The direct precipitation model suggests Mn carbonate nucleation and accumulation in anoxic waters. If that is the case, the carbonate would be expected to show consistently low I/(Ca + Mg) values. This is because iodate is prevalent in oxygenated seawater but significantly diminished in reducing seawater (Wong and Brewer 1977), while only iodate is incorporated into the carbonate lattice (Lu *et al.* 2010; Hashim *et al.* 2022). Hence, carbonate-associated iodine (expressed as I/(Ca + Mg)) can potentially track iodate concentrations and hence redox conditions under which carbonate minerals precipitated. The I/(Ca + Mg) values of more than half of our samples are over the Precambrian baseline of 0.5 μmol/mol (Lu *et al.* 2017; Fig. 3). No significant contamination is observed, as supported by relatively high carbonate contents (average 84%) and its absence of covariation with I/(Ca + Mg) (Fig. S2). There are also no significant covariations between Mn/Sr, $\delta^{18}O$ and I/(Ca + Mg) in the lower member (Fig. S2). Nevertheless, the significant variability of I/(Ca + Mg) observed in the lower member may indicate iodine loss during early diagenesis (Hardisty *et al.* 2017). In combination with the low partition coefficient of iodate in dolostone (Hashim *et al.* 2022), these variable but overall modest I/(Ca + Mg) values (0.63 ± 0.44 μmol/mol) provide minimum estimates of seawater iodate levels. This supports dolostone deposition in a non-zero oxygen environment. Additionally, carbonate REE patterns could provide further nuance about the fluid characteristics during deposition. The Daizhuangzi carbonates display non-seawater-like REE patterns characterized by light and middle REE enrichment (Fig. 3). The absence of strong covariation between REE and Al contents suggests that these REE patterns are unlikely to result from detrital contamination (Fig. S3). In comparison, the late Ediacaran Gaoyan Mn carbonates exhibit seawater-like REE patterns, which are interpreted to reflect direct precipitation in seawater (Gao *et al.* 2021). Together with elevated Mn (and also Fe) contents, the non-seawater-like REE patterns in Daizhuangzi carbonates are probably derived from incorporation of REE released from the reductive dissolution of Mn/Fe oxides during early diagenesis (Zhang and Shields 2023).

The Wafangzi deposit is one of the largest ferromanganese ore deposits in North China and is correlated with the Daizhuangzi member of the Tieling Formation (Fan *et al.* 1999). A recent study suggests that Mn carbonates in the Wafangzi deposit are derived from diagenetic reduction of precursor Mn/Fe oxides during early diagenesis (Yan *et al.* 2024), which is in line with our interpretation. The diagenetic reduction of Mn/Fe oxides is commonly accompanied by organic matter decomposition and release of ^{13}C-depleted bicarbonate. Diagenetic Mn carbonates are thus often characterized by negative $\delta^{13}C$ values that may reveal a negative covariation with Mn contents (Roy 2006). The Mn carbonates at Wafangzi have significantly higher Mn contents (generally above 20%) and relatively lower $\delta^{13}C$ values ranging between −8 and −4‰ (Yan *et al.* 2024). In contrast, the Daizhuangzi carbonates at Jixian have

relatively lower Mn contents and higher $\delta^{13}C$ values showing an increasing trend from −2.3 to −0.7‰ (Fig. 3). Together with the absence of covariation between $\delta^{13}C$ and diagenetic parameters (Fig. S4), these observations suggest that the stratigraphic trend of increasing $\delta^{13}C$ values in the Daizhuangzi member could be primary. Indeed, comparable $\delta^{13}C$ trends are evident across sections, suggesting that this stratigraphic pattern may serve as a useful tool for future chemostratigraphic correlations.

The Laohuding member of the Tieling Formation

Evaluation of diagenetic effects

Carbonate rocks serve as an important sedimentary archive, which can preserve useful deep-time geochemical signals, but they are also prone to diagenetic alteration. Therefore, it is of great importance to evaluate diagenetic effects before any proper interpretation of carbonate-based geochemical proxies can be attempted. For the purpose of this study, we mainly focus on the diagenetic effects on carbonate $\delta^{13}C$, REE and I/(Ca + Mg) signals.

The $\delta^{13}C$ values of the Laohuding member increase from around −0.4 to +1.0‰ in the lower part and then show a broadly decreasing trend to around −0.9‰ towards its top (Fig. 3). Several lines of evidence indicate that this relatively consistent stratigraphic trend is unlikely to be caused by diagenesis. The elemental exchange during meteoric diagenesis tends to increase Mn/Sr ratios and decrease $\delta^{13}C$ and $\delta^{18}O$ values of carbonates (Brand and Veizer 1980). For this reason, it has been proposed that carbonate samples with Mn/Sr < 10 and $\delta^{18}O > -10$‰ are more likely to preserve primary $\delta^{13}C$ signals (Kaufman and Knoll 1995). Nearly all our carbonate samples have $\delta^{18}O$ of greater than −10‰ (Fig. 3), while Mn/Sr ratios are mostly lower than 5 in our samples (Supplementary data). Although such absolute cut-offs may not be applicable to every study, cross-plots indicate that our $\delta^{13}C$ values do not covary significantly with Mn/Sr and $\delta^{18}O$ (Fig. S4). Dolomitization can potentially retain, increase or decrease primary $\delta^{13}C$ values (Swart 2015; Zhang *et al.* 2024*b*). However, the Mg/Ca ratios of our samples are mostly lower than 0.1 with sporadic Mg/Ca spikes throughout the section (Fig. 3). There is also no significant covariation between $\delta^{13}C$ and Mg/Ca (Fig. S4). Moreover, the increasing $\delta^{13}C$ trend through the lower part followed by steady decrease in the upper part is broadly consistent with previous $\delta^{13}C$ studies (Fig. 4). Therefore, we suggest that our measured $\delta^{13}C$ trend for the Laohuding carbonates broadly reflects secular changes to local ocean dissolved inorganic carbon.

Carbonate-bound REE is considered to be able to preserve the seawater REE signal and hence be an informative proxy for palaeo-seawater chemistry (Webb and Kamber 2000; Nothdurft *et al.* 2004). Nevertheless, interpretation of carbonate REE patterns should consider the potential influence of non-carbonate phase contamination during leaching and elemental exchange during diagenesis (reviewed in Zhang and Shields 2022). Non-carbonate phases are generally characterized by distinct REE patterns and high REE concentrations and so the inadvertent leaching of non-carbonate phases may obscure primary signals (Zhang *et al.* 2015; Tostevin *et al.* 2016; Cao *et al.* 2020). Carbonate REE could also potentially be altered during diagenesis, the influence of which is most easily discernible from the REE pattern (Zhang and Shields 2023). The Laohuding carbonate samples are relatively pure with an average carbonate content of 91% (Supplementary data). Moreover, we adopted a sequential leaching approach to avoid strongly attacking non-carbonate phases (see Methods). The general seawater-like REE patterns (Fig. 3) and absence of strong covariations between REE contents and major elements (Fig. S3) suggest limited contamination and overall good preservation of seawater signals. For this study, we screened the REE data based on the following criteria: Y/Ho > 35, $Pr_N/Yb_N < 1$, positive La and Gd anomalies (>1), and ∑REE < 50 ppm (Ling *et al.* 2013; Zhang and Shields 2022). The screening strategy does not affect the stratigraphic trend and reduces the data dispersion. The screened dataset shows that Ce/Ce* values of the Laohuding member decrease from ~0.9 to ~0.65 in the lower part and then remain relatively stable at ~0.70 before gradually increasing to around 0.9 (Fig. 3).

Carbonate I/(Ca + Mg) values reveal a clear stratigraphic trend, whereby I/(Ca + Mg) decreases from 0.90 μmol/mol to values below 0.5 μmol/mol in the lower part and remains consistently low before increasing to 2.05 μmol/mol near the top (Fig. 3). Contamination from organic matter and/or phosphate minerals during leaching may artificially increase I/(Ca + Mg) values (Zhang

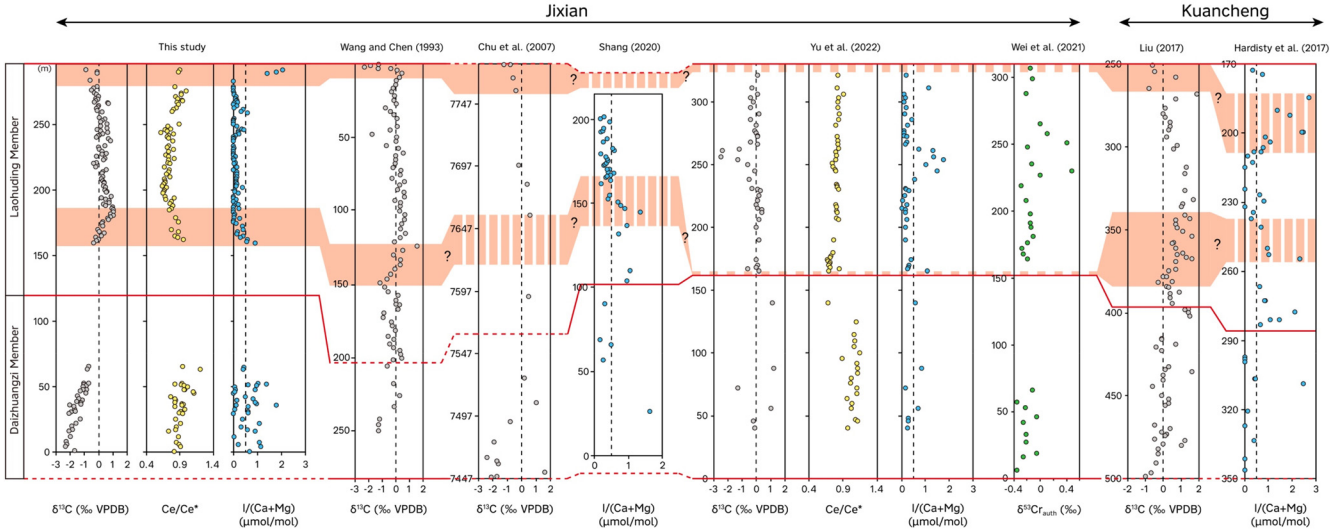

Fig. 4. Stratigraphic correlation of geochemical data from the Tieling Formation at Jixian and Kuancheng. Red lines represent lithostratigraphic unit boundaries separating members and the Tieling Formation from underlying and overlying formations. Solid red lines represent boundaries shown in the original studies, while dashed red lines represent boundaries inferred from lithology and/or Mn contents. Shaded bands represent correlations based on $\delta^{13}C$ and I/(Ca + Mg) trends, while discontinuous bands indicate correlations with high uncertainty that require further verification. Carbonate $\delta^{13}C$, Ce/Ce*, I/(Ca + Mg) and $\delta^{53}Cr$ data are marked as grey, yellow, blue and green circles, respectively. Source: Wang and Chen (1993), Chu *et al.* (2007), Liu (2017), Hardisty *et al.* (2017), Shang (2020), Wei *et al.* (2021) and Yu *et al.* (2022).

et al. 2024*a*), but as mentioned above, our carbonate samples are relatively pure, implying negligible contribution from non-carbonate phases. The absence of covariation between I/(Ca + Mg) and carbonate content also suggests limited detrital contamination (Fig. S2). Diagenetic processes generally lead to iodine loss from carbonate rocks, and bulk carbonate I/(Ca + Mg) values are generally considered to place minimal constraints on local–regional iodate availability (Hardisty *et al.* 2017; Lu *et al.* 2020). This is mainly because iodate reduces rapidly to iodide in reducing diagenetic fluids, while only iodate is incorporated into the carbonate lattice (Lu *et al.* 2010; Hashim *et al.* 2022). There are no significant covariations between Mn/Sr, $\delta^{18}O$ and I/(Ca + Mg) in our samples (Fig. S2), indicating limited influence of meteoric diagenesis. Dolomitized samples appear to contain relatively lower I/(Ca + Mg) values (or below the detection limit) compared with adjacent limestone samples, providing support for substantial iodine loss during dolomitization. Nevertheless, the samples are characterized by overall low Mg/Ca ratios that show no covariation with I/(Ca + Mg) (Fig. S2). Taken together, the stratigraphic trend of I/(Ca + Mg) values is unlikely to be due to diagenesis.

Shallow-marine redox dynamics

Our I/(Ca + Mg) data reveal a minor peak in the lower part of the upper member corresponding to rising $\delta^{13}C$ values (Figs 3, 4). Based on the lithostratigraphy, this minor peak could be potentially correlated with the similar intervals at Jixian (Shang 2020) and Kuancheng (Hardisty *et al.* 2017; Fig. 4), although such a correlation needs to be further substantiated by $\delta^{13}C$ data. Conversely, this minor I/(Ca + Mg) peak and positive $\delta^{13}C$ shift are not evident in Yu *et al.* (2022), while they reported a transient peak of I/(Ca + Mg) coincident with a negative $\delta^{13}C$ excursion from the middle part (Yu *et al.* 2022), which are not apparent in our study (Fig. 4). This discrepancy is perhaps because the intervals were missed during sampling in the field. We also observe another I/(Ca + Mg) peak near the top of the upper member of the Tieling Formation, which corresponds to decreasing $\delta^{13}C$ values (Figs 3, 4). While the decreasing trend of $\delta^{13}C$ near the top of the Tieling Formation appears to be reproducible at multiple sites (Fig. 4), the lack of integrated $\delta^{13}C$ and I/(Ca + Mg) profiles makes it difficult to correlate this I/(Ca + Mg) peak. Again, if we accept the lithostratigraphic column of Hardisty *et al.* (2017), this I/(Ca + Mg) peak is potentially correlated with that observed at Kuancheng (Fig. 4). Nevertheless, it should be noted that those high I/(Ca + Mg) values at Kuancheng have been previously correlated with the transient I/(Ca + Mg) peak in the middle part of the upper member at Jixian (Yu *et al.* 2022). Such a correlation is based on the occurrence of stromatolites (Yu *et al.* 2022). However, the lithostratigraphic column for Kuancheng invoked by Yu *et al.* (2022) is from outcrop, whereas the I/(Ca + Mg) data at Kuancheng are obtained from the JQ2 well (Hardisty *et al.* 2017). Such a correlation thus remains ambiguous. Overall, our I/(Ca + Mg) dataset suggests that there was greater iodate (and possibly oxygen) availability in seawater during deposition of the lower and top parts of the upper member of the Tieling Formation.

The Ce anomaly provides an independent constraint for shallow seawater redox conditions. In modern oxic seawater, cerium is readily oxidized to relatively insoluble Ce(IV) mainly on the surface of Mn oxides, resulting in relative Ce depletion (i.e. a negative Ce anomaly; De Baar *et al.* 1985; Sholkovitz *et al.* 1994; Ohta and Kawabe 2001). With increasing water depth in the shallow oxic water column, the magnitude of the Ce anomaly continues to increase until equilibrium is reached (Sholkovitz *et al.* 1994), while release of REE from settling particles in deeper suboxic/anoxic seawater commonly leads to no Ce anomaly or a positive Ce anomaly (Tostevin *et al.* 2016). Our Ce/Ce* data are mostly lower than 0.9 (Fig. 3), suggesting that the studied interval was largely deposited under oxic conditions. The variation of Ce/Ce* values from high through low to high again closely resembles the interpreted sea-level change (Figs 2, 3), implying a water depth control. In support of this, consistently low I/(Ca + Mg) values largely correspond to low Ce/Ce* (Fig. 3), which seems counterintuitive at first glance. Such a coupling is mainly because in addition to the oxygen level, carbonate I/(Ca + Mg) is also affected by the proximity to an oxycline (Lu *et al.* 2020). Due to the relatively slow oxidation kinetics of iodide to iodate, I/(Ca + Mg) values are typically low above oxygen minimum zones or a shallow oxycline (Z. Lu *et al.* 2016; W. Lu *et al.*, 2018). For example, the coupling of low Ce/Ce* and I/(Ca + Mg) values is also observed in the late Paleozoic (Zhang and Shields 2022), during which atmospheric oxygen is considered to be close to modern-day levels (Krause *et al.* 2018). In combination, one plausible explanation for the stratigraphic trends of the two redox proxies is that they are probably induced by sea-level changes and the redox chemocline was perhaps close to or below the fair-weather wave base during deposition of the upper member.

Implications for Mesoproterozoic oxygenation

Carbonate I/(Ca + Mg) values have been widely used to infer 'oxygenation events' during the Mesoproterozoic (or on a wider timescale the mid-Proterozoic). The I/(Ca + Mg) value of 0.5 μmol/mol is inferred to be the baseline for Precambrian carbonates based on statistical analysis of published data (Hardisty *et al.* 2017; Lu *et al.* 2017; Shang *et al.* 2019). Therefore, I/(Ca + Mg) values greater than the baseline have been commonly invoked to support 'oxygenation events'. However, our data suggest that I/(Ca + Mg) values lower than 0.5 μmol/mol do not necessarily indicate low-oxygen seawaters (Fig. 3). This is not surprising as such low values can be found above the chemocline even under modern oxygenated ocean–atmosphere conditions (Z. Lu *et al.* 2016, 2020; W. Lu *et al.*, 2018). It should be noted that our findings do not nullify the indication of high I/(Ca + Mg) for high oxygen availability, and high I/(Ca + Mg) values in deeper water deposits probably continue to provide evidence for oxygenation (e.g. Shang *et al.* 2019). Instead, it is necessary to examine whether the stratigraphic variation of I/(Ca + Mg) is caused by a natural iodate gradient in the water column or an oxygenation event (i.e. an overall increase in oxygen contents). In this regard, our study indicates that the combination of Ce anomalies with I/(Ca + Mg) ratios can constrain shallow seawater redox conditions better.

The Ce anomaly data from both the lower and upper members of the Tieling Formation indicate the operation of Mn cycling. Although oxygen-independent pathways of Mn oxidation exist such as through anoxygenic photosynthesis (Daye *et al.* 2019) or abiotically photochemical reactions (Liu *et al.* 2020), these Mn oxidation pathways are considered unlikely to exert appreciable controls on geological records (Lyons *et al.* 2020; Robbins *et al.* 2023). In contrast, due to the high redox potential of Mn(II)/Mn(IV), active Mn cycling is considered to imply a minimum of ~10 μM O_2 (Tostevin *et al.* 2016). The significant negative Ce anomalies (~0.6–0.7) complemented with relatively high I/(Ca + Mg) values (~1–2 μmol/mol) suggest that the maximum oxygen concentrations may have been significantly greater than 10 μM. Given present age constraints of the Tieling Formation, such an oxygenated shallow ocean could have persisted on the order of tens of million years. The question remains as to whether this oxygenated seawater condition is globally or even regionally traceable. Whereas redox proxy data for the upper member so far mostly come from Jixian, the general development of Mn-rich carbonates in the lower member of the Tieling Formation supports at least a regionally oxygenated shallow seawater column (Yan *et al.*

2024). Outside the North China Craton, considerable Mn deposits have also been reported from the *c.* 1.45 Ga Ullawarra Formation on the Pilbara Craton (Spinks *et al.* 2023). High $\delta^{15}N$ values (up to +5‰) indicating aerobic nitrogen cycling have also been reported from the *c.* 1.45 Ga lower Belt Supergroup (Stüeken 2013). These observations suggest that seawater may have been significantly oxygenated on a global scale, but sparse accurate age constraints from these formations preclude any direct comparison, warranting further study.

Conclusions

We present a relatively high-resolution multiproxy dataset including carbonate $\delta^{13}C$, REE and I/(Ca + Mg) data from the Tieling Formation at Jixian. The $\delta^{13}C$ values reveal systematic stratigraphic trends, which increase from −2.3 to −0.7‰ in the lower member, and from −0.4 to +1.0‰ followed by a decrease to −0.9‰ in the upper member. The lower member Mn-rich carbonates exhibit non-seawater-like REE patterns but relatively high I/(Ca + Mg) values (up to 1.78 μmol/mol). These geochemical signals are interpreted to be indicative of early diagenetic reduction of primary Mn oxides. For the upper member, negative Ce anomalies (mainly 0.6–0.9) and I/(Ca + Mg) values (0–2.05 μmol/mol) display coupled stratigraphic variation, which we attribute to sea-level change rather than oxygenation. Our study cautions that low I/(Ca + Mg) or high Ce/Ce* values alone might not necessarily indicate an overall low-oxygen water column but may be affected by chemocline depth or sea-level change. Future studies combining the two redox proxies together can better constrain the shallow seawater redox conditions. Furthermore, the geochemical data from the Tieling Formation support vigorous oxidative Mn cycling, suggesting that an oxygenated shallow ocean probably persisted for multimillion years in the Mesoproterozoic. Regional development of Mn-rich carbonates in the Yanliao Basin and the documentation of Mn deposits in the ∼1.45 Ga Ullawarra Formation of Australia imply perhaps a widespread oxygenation that warrants further study.

Scientific editing by Fengqi Zhang

Acknowledgements KZ acknowledges support from the University College London Faculty Dean's Prize and China Scholarship Council. We thank Hanqing Zhao for assistance during fieldwork. We are grateful to Gary Tarbuck, Anne-Lise Jourdan and Jim Davy for their technical support. We thank Shuan-Hong Zhang and the anonymous reviewer for constructive review comments that improved the manuscript.

Author contributions **KZ**: investigation (lead), visualization (lead), writing – original draft (lead), writing – review & editing (equal); **LM**: resources (equal), writing – review & editing (equal); **SZ**: resources (equal); **YZ**: resources (equal), writing – review & editing (equal); **GS**: conceptualization (lead), funding acquisition (lead), resources (equal), supervision (lead), writing – review & editing (equal)

Funding This work was funded by the Natural Environment Research Council (NE/R010129/1 to GS).

Competing interests The authors declare that they have no known competing financial interests or personal relationships that could have appeared to influence the work reported in this paper.

Data availability All data generated or analysed during this study are included in this published article (and if present, its supplementary information files).

References

Bekker, A., Holland, H.D. *et al.* 2004. Dating the rise of atmospheric oxygen. *Nature*, **427**, 117–120, https://doi.org/10.1038/nature02260

Brand, U. and Veizer, J. 1980. Chemical diagenesis of a multicomponent carbonate system–1: trace elements. *Journal of Sedimentary Research*, **50**, 987–998, https://doi.org/10.1306/212F7BB7-2B24-11D7-8648000102C1865D

Brasier, M.D. and Lindsay, J.F. 1998. A billion years of environmental stability and the emergence of eukaryotes: new data from northern Australia. *Geology*, **26**, 555–558, https://doi.org/10.1130/0091-7613(1998)026<0555:ABYOES>2.3.CO;2

Buick, R., Des Marais, D.J. and Knoll, A.H. 1995. Stable isotopic compositions of carbonates from the Mesoproterozoic Bangemall group, northwestern Australia. *Chemical Geology*, **123**, 153–171, https://doi.org/10.1016/0009-2541(95)00049-R

Calvert, S.E. and Pedersen, T.F. 1996. Sedimentary geochemistry of manganese: implications for the environment of formation of manganiferous black shales. *Economic Geology*, **91**, 36–47, https://doi.org/10.2113/gsecongeo.91.1.36

Canfield, D.E. 2005. The early history of atmospheric oxygen: Homage to Robert M. Garrels. *Annual Review of Earth and Planetary Sciences*, **33**, 1–36, https://doi.org/10.1146/annurev.earth.33.092203.122711

Canfield, D.E., Zhang, S. *et al.* 2018. Highly fractionated chromium isotopes in Mesoproterozoic-aged shales and atmospheric oxygen. *Nature Communications*, **9**, 1–11, https://doi.org/10.1038/s41467-018-05263-9

Cao, C., Liu, X.-M., Bataille, C.P. and Liu, C. 2020. What do Ce anomalies in marine carbonates really mean? A perspective from leaching experiments. *Chemical Geology*, **532**, 119413, https://doi.org/10.1016/j.chemgeo.2019.119413

Chu, X., Zhang, T., Zhang, Q. and Lyons, T.W. 2007. Sulfur and carbon isotope records from 1700 to 800 Ma carbonates of the Jixian section, northern China: implications for secular isotope variations in Proterozoic seawater and relationships to global supercontinental events. *Geochimica et Cosmochimica Acta*, **71**, 4668–4692, https://doi.org/10.1016/j.gca.2007.07.017

Dahl, T.W., Hammarlund, E.U. *et al.* 2010. Devonian rise in atmospheric oxygen correlated to the radiations of terrestrial plants and large predatory fish. *Proceedings of the National Academy of Sciences*, **107**, 17911–17915, https://doi.org/10.1073/pnas.1011287107

Daye, M., Klepac-Ceraj, V. *et al.* 2019. Light-driven anaerobic microbial oxidation of manganese. *Nature*, **576**, 311–314, https://doi.org/10.1038/s41586-019-1804-0

De Baar, H.J.W., Bacon, M.P., Brewer, P.G. and Bruland, K.W. 1985. Rare earth elements in the Pacific and Atlantic Oceans. *Geochimica et Cosmochimica Acta*, **49**, 1943–1959, https://doi.org/10.1016/0016-7037(85)90089-4

Fan, D., Ye, J. and Li, J. 1999. Geology, mineralogy, and geochemistry of the Middle Proterozoic Wafangzi ferromanganese deposit, Liaoning Province, China. *Ore Geology Reviews*, **15**, 31–53, https://doi.org/10.1016/S0169-1368(99)00013-X

Gao, Z., Zhu, X., Wang, D., Pan, C., Yan, B. and Li, J. 2021. Insights into hydrothermal controls and processes leading to the formation of the Late Ediacaran Gaoyan stratiform manganese-carbonate deposit, Southwest China. *Ore Geology Reviews*, **139**, https://doi.org/10.1016/j.oregeorev.2021.104524

Guo, W., Su, W. *et al.* 2019. Zircon U-Pb dating and Hf isotopes of K-bentonites from the Tieling Formation in a new exposure of the Jixian Section, Tianjin, North China Craton. *Acta Petrologica Sinica*, **35**, 2433–2454, https://doi.org/10.18654/1000-0569/2019.08.08

Hardisty, D.S., Lu, Z. *et al.* 2017. Perspectives on Proterozoic surface ocean redox from iodine contents in ancient and recent carbonate. *Earth and Planetary Science Letters*, **463**, 159–170, https://doi.org/10.1016/j.epsl.2017.01.032

Hashim, M.S., Burke, J.E., Hardisty, D.S. and Kaczmarek, S.E. 2022. Iodine incorporation into dolomite: experimental constraints and implications for the iodine redox proxy and Proterozoic Ocean. *Geochimica et Cosmochimica Acta*, **338**, 365–381, https://doi.org/10.1016/j.gca.2022.10.027

Herndon, E.M., Havig, J.R., Singer, D.M., McCormick, M.L. and Kump, L.R. 2018. Manganese and iron geochemistry in sediments underlying the redox-stratified Fayetteville Green Lake. *Geochimica et Cosmochimica Acta*, **231**, 50–63, https://doi.org/10.1016/j.gca.2018.04.013

Hu, J., Li, Z., Gong, W., Hu, G. and Dong, X. 2016. Meso-Neoproterozoic stratigraphic and tectonic framework of the North China Craton. *In:* Zhai, M., Zhao, Y. and Zhao, T. (eds) *Main Tectonic Events and Metallogeny of the North China Craton*. Springer, 393–422, https://doi.org/10.1007/978-981-10-1064-4_15

Kaufman, A.J. and Knoll, A.H. 1995. Neoproterozoic variations in the C-isotopic composition of seawater: stratigraphic and biogeochemical implications. *Precambrian Research*, **73**, 27–49, https://doi.org/10.1016/0301-9268(94)00070-8

Krause, A.J., Mills, B.J.W., Zhang, S., Planavsky, N.J., Lenton, T.M. and Poulton, S.W. 2018. Stepwise oxygenation of the Paleozoic atmosphere. *Nature Communications*, **9**, 1–10, https://doi.org/10.1038/s41467-018-06383-y

Lawrence, M.G. and Kamber, B.S. 2006. The behaviour of the rare earth elements during estuarine mixing-revisited. *Marine Chemistry*, **100**, 147–161, https://doi.org/10.1016/j.marchem.2005.11.007

Li, H.K., Su, W.B. *et al.* 2014. The first precise age constraints on the Jixian System of the Meso- to Neoproterozoic Standard Section of China; SHRIMP

zircon U-Pb dating of bentonites from the Wumishan and Tiding formations in the Jixian Section, North China Craton. *Acta Petrologica Sinica*, **30**, 2999–3012, https://doi.org/10.0000/5694fa73c5504a3f88413737eee7cc30

Ling, H.-F., Chen, X., Li, D., Wang, D., Shields-Zhou, G.A. and Zhu, M. 2013. Cerium anomaly variations in Ediacaran–earliest Cambrian carbonates from the Yangtze Gorges area, South China: implications for oxygenation of coeval shallow seawater. *Precambrian Research*, **225**, 110–127, https://doi.org/10.1016/j.precamres.2011.10.011

Liu, G.C. 2017. *Carbon Isotope Compositions in Mesoproterozoic Samples from North China Platform and Paleo-Environmental Changes*. China University of Petroleum, Beijing.

Liu, W., Hao, J., Elzinga, E.J., Piotrowiak, P., Nanda, V., Yee, N. and Falkowski, P.G. 2020. Anoxic photogeochemical oxidation of manganese carbonate yields manganese oxide. *Proceedings of the National Academy of Sciences of the United States of America*, **117**, 22698–22704, https://doi.org/10.1073/pnas.2002175117

Lu, S., Zhao, G., Wang, H. and Hao, G. 2008. Precambrian metamorphic basement and sedimentary cover of the North China Craton: a review. *Precambrian Research*, **160**, 77–93, https://doi.org/10.1016/j.precamres.2007.04.017

Lu, Z., Jenkyns, H.C. and Rickaby, R.E.M. 2010. Iodine to calcium ratios in marine carbonate as a paleo-redox proxy during oceanic anoxic events. *Geology*, **38**, 1107–1110, https://doi.org/10.1130/G31145.1

Lu, Z., Hoogakker, B.A.A. *et al.* 2016. Oxygen depletion recorded in upper waters of the glacial Southern Ocean. *Nature Communications*, **7**, 11146, https://doi.org/10.1038/ncomms11146

Lu, W., Wörndle, S. *et al.* 2017. Iodine proxy evidence for increased ocean oxygenation during the Bitter Springs Anomaly. *Geochemical Perspectives Letters*, **5**, 53–57, https://doi.org/10.7185/geochemlet.1746

Lu, W., Ridgwell, A. *et al.* 2018. Late inception of a resiliently oxygenated upper ocean. *Science*, **177**, 174–177, https://doi.org/10.1126/science.aar5372

Lu, Z., Lu, W., Rickaby, R.E.M. and Thomas, E. 2020. *Earth History of Oxygen and the IprOxy*. Cambridge University Press, https://doi.org/10.1017/9781108688604

Luo, J., Long, X. *et al.* 2021. Pulsed oxygenation events drove progressive oxygenation of the early Mesoproterozoic ocean. *Earth and Planetary Science Letters*, **559**, https://doi.org/10.1016/j.epsl.2021.116754

Lyons, T.W., Reinhard, C.T. and Planavsky, N.J. 2014. The rise of oxygen in Earth's early ocean and atmosphere. *Nature*, **506**, 307–315, https://doi.org/10.1038/nature13068

Lyons, T.W., Diamond, C.W. and Konhauser, K.O. 2020. Shedding light on manganese cycling in the early oceans. *Proceedings of the National Academy of Sciences*, **117**, 25960–25962, https://doi.org/10.1073/pnas.2016447117

Lyons, T.W., Diamond, C.W., Planavsky, N.J., Reinhard, C.T. and Li, C. 2021. Oxygenation, life, and the planetary system during Earth's middle history: an overview. *Astrobiology*, **21**, 906–923, https://doi.org/10.1089/ast.2020.2418

Lyu, D., Deng, Y. *et al.* 2021. Using cyclostratigraphic evidence to define the unconformity caused by the Mesoproterozoic Qinyu Uplift in the North China Craton. *Journal of Asian Earth Sciences*, **206**, 104608, https://doi.org/10.1016/j.jseaes.2020.104608

Maynard, J.B. 2010. The chemistry of manganese ores through time: a signal of increasing diversity of earth-surface environments. *Economic Geology*, **105**, 535–552, https://doi.org/10.2113/gsecongeo.105.3.535

Mei, M., Yang, F., Gao, J. and Meng, Q. 2008. Glauconites formed in the high-energy shallow-marine environment of the late mesoproterozoic: case study from Tieling Formation at Jixian Section in Tianjin, North China. *Earth Science Frontiers*, **15**, 146–158, https://doi.org/10.1016/S1872-5791(08)60048-2

Meng, L., Shi, X. *et al.* 2025. A prominent oxygenation event in the late Mesoproterozoic broke the calm of the second half of the 'Boring Billion'. *Palaeogeography, Palaeoclimatology, Palaeoecology*, **662**, 112752, https://doi.org/10.1016/j.palaeo.2025.112752

Miao, L., Moczydłowska, M. and Zhu, M. 2021. A diverse organic-walled microfossil assemblage from the Mesoproterozoic Xiamaling Formation, North China. *Precambrian Research*, **360**, 106235, https://doi.org/10.1016/j.precamres.2021.106235

Miao, L., Yin, Z., Knoll, A.H., Qu, Y. and Zhu, M. 2024. 1.63-billion-year-old multicellular eukaryotes from the Chuanlinggou Formation in North China. *Science Advances*, **10**, 1–12, https://doi.org/10.1126/sciadv.adk3208

Mukherjee, I. and Large, R.R. 2016. Pyrite trace element chemistry of the Velkerri Formation, Roper Group, McArthur Basin: evidence for atmospheric oxygenation during the Boring Billion. *Precambrian Research*, **281**, 13–26, https://doi.org/10.1016/j.precamres.2016.05.003

Nothdurft, L.D., Webb, G.E. and Kamber, B.S. 2004. Rare earth element geochemistry of Late Devonian reefal carbonates, Canning Basin, Western Australia: confirmation of a seawater REE proxy in ancient limestones. *Geochimica et Cosmochimica Acta*, **68**, 263–283, https://doi.org/10.1016/S0016-7037(03)00422-8

Och, L.M. and Shields-Zhou, G.A. 2012. The Neoproterozoic oxygenation event: environmental perturbations and biogeochemical cycling. *Earth-Science Reviews*, **110**, 26–57, https://doi.org/10.1016/j.earscirev.2011.09.004

Ohta, A. and Kawabe, I. 2001. REE(III) adsorption onto Mn dioxide (δ-MnO_2) and Fe oxyhydroxide: Ce(III) oxidation by δ-MnO_2. *Geochimica et Cosmochimica Acta*, **65**, 695–703, https://doi.org/10.1016/S0016-7037(00)00578-0

Pourmand, A., Dauphas, N. and Ireland, T.J. 2012. A novel extraction chromatography and MC-ICP-MS technique for rapid analysis of REE, Sc and Y: revising CI-chondrite and Post-Archean Australian Shale (PAAS) abundances. *Chemical Geology*, **291**, 38–54, https://doi.org/10.1016/j.chemgeo.2011.08.011

Robbins, L.J., Fakhraee, M. *et al.* 2023. Manganese oxides, Earth surface oxygenation, and the rise of oxygenic photosynthesis. *Earth-Science Reviews*, **239**, https://doi.org/10.1016/j.earscirev.2023.104368

Roy, S. 2006. Sedimentary manganese metallogenesis in response to the evolution of the Earth system. *Earth-Science Reviews*, **77**, 273–305, https://doi.org/10.1016/j.earscirev.2006.03.004

Shang, M.H. 2020. *Redox Evolution of the Mesoproterozoic Ocean Indicated by Carbonate-Associated Iodine Abundance*. China University of Geosciences, Beijing.

Shang, M., Tang, D., Shi, X., Zhou, L., Zhou, X., Song, H. and Jiang, G. 2019. A pulse of oxygen increase in the early Mesoproterozoic ocean at ca. 1.57–1.56 Ga. *Earth and Planetary Science Letters*, **527**, 115797, https://doi.org/10.1016/j.epsl.2019.115797

Sholkovitz, E.R., Landing, W.M. and Lewis, B.L. 1994. Ocean particle chemistry: the fractionation of rare earth elements between suspended particles and seawater. *Geochimica et Cosmochimica Acta*, **58**, 1567–1579, https://doi.org/10.1016/0016-7037(94)90559-2

Sperling, E.A., Rooney, A.D. *et al.* 2014. Redox heterogeneity of subsurface waters in the Mesoproterozoic ocean. *Geobiology*, **12**, 373–386, https://doi.org/10.1111/gbi.12091

Spinks, S.C., Sperling, E.A. *et al.* 2023. Mesoproterozoic surface oxygenation accompanied major sedimentary manganese deposition at 1.4 and 1.1 Ga. *Geobiology*, **21**, 28–43, https://doi.org/10.1111/gbi.12524

Stüeken, E.E. 2013. A test of the nitrogen-limitation hypothesis for retarded eukaryote radiation: nitrogen isotopes across a Mesoproterozoic basinal profile. *Geochimica et Cosmochimica Acta*, **120**, 121–139, https://doi.org/10.1016/j.gca.2013.06.002

Su, W., Li, H., Huff, W.D., Ettensohn, F.R., Zhang, S., Zhou, H. and Wan, Y. 2010. SHRIMP U-Pb dating for a K-bentonite bed in the Tieling Formation, North China. *Chinese Science Bulletin*, **55**, 3312–3323, https://doi.org/10.1007/s11434-010-4007-5

Swart, P.K. 2015. The geochemistry of carbonate diagenesis: the past, present and future. *Sedimentology*, **62**, 1233–1304, https://doi.org/10.1111/sed.12205

Tang, D., Shi, X., Wang, X. and Jiang, G. 2016. Extremely low oxygen concentration in mid-Proterozoic shallow seawaters. *Precambrian Research*, **276**, 145–157, https://doi.org/10.1016/j.precamres.2016.02.005

Tang, D., Shi, X., Ma, J., Jiang, G., Zhou, X. and Shi, Q. 2017. Formation of shallow-water glaucony in weakly oxygenated Precambrian ocean: An example from the Mesoproterozoic Tieling Formation in North China. *Precambrian Research*, **294**, 214–229, https://doi.org/10.1016/j.precamres.2017.03.026

Tostevin, R., Wood, R.A. *et al.* 2016. Low-oxygen waters limited habitable space for early animals. *Nature Communications*, **7**, 12818, https://doi.org/10.1038/ncomms12818

Wang, K.F. and Chen, J.S. 1993. Constraints on the stable isotopic composition of sedimentary carbonates from the Tieling Formation in the Yanshan region. *Geochimica*, **1**, 10–17.

Webb, G.E. and Kamber, B.S. 2000. Rare earth elements in Holocene reefal microbialites: a new shallow seawater proxy. *Geochimica et Cosmochimica Acta*, **64**, 1557–1565, https://doi.org/10.1016/S0016-7037(99)00400-7

Wei, W., Frei, R. *et al.* 2021. A transient swing to higher oxygen levels in the atmosphere and oceans at ∼1.4 Ga. *Precambrian Research*, **354**, 106058, https://doi.org/10.1016/j.precamres.2020.106058

Wei, W., Wang, H., Zhang, S., Dong, L.-H., Li, D. and Huang, F. 2025. Dynamic redox evolution in the middle-late Mesoproterozoic oceans. *Chemical Geology*, **679**, 122685, https://doi.org/10.1016/j.chemgeo.2025.122685

Wittkop, C., Swanner, E.D. *et al.* 2020. Evaluating a primary carbonate pathway for manganese enrichments in reducing environments. *Earth and Planetary Science Letters*, **538**, https://doi.org/10.1016/j.epsl.2020.116201

Wong, G.T.F. and Brewer, P.G. 1977. The marine chemistry of iodine in anoxic basins. *Geochimica et Cosmochimica Acta*, **41**, 151–159, https://doi.org/10.1016/0016-7037(77)90195-8

Yan, H., Xu, L. *et al.* 2024. Mineralogy of the 1.45 Ga Wafangzi manganese deposit in North China: implications for pulsed Mesoproterozoic oxygenation events. *American Mineralogist*, **109**, 764–784, https://doi.org/10.2138/am-2022-8919

Yang, S., Kendall, B., Lu, X., Zhang, F. and Zheng, W. 2017. Uranium isotope compositions of mid-Proterozoic black shales: evidence for an episode of increased ocean oxygenation at 1.36 Ga and evaluation of the effect of post-depositional hydrothermal fluid flow. *Precambrian Research*, **298**, 187–201, https://doi.org/10.1016/j.precamres.2017.06.016

Yu, Y., Chen, Y., Li, D. and Su, J. 2022. A transient oxygen increase in the Mesoproterozoic ocean at ∼1.44 Ga: geochemical evidence from the Tieling Formation, North China Platform. *Precambrian Research*, **369**, 106527, https://doi.org/10.1016/j.precamres.2021.106527

Yu, Y., Chen, Y., Li, D. and Xia, B. 2025. Pulsed oxygenation events at ∼ 1.44–1.43 Ga: evidence from the Tieling Formation in the North China Platform. *Precambrian Research*, **419**, 107723, https://doi.org/10.1016/j.precamres.2025.107723

Zhai, M., Hu, B., Zhao, T., Peng, P. and Meng, Q. 2015. Late Paleoproterozoic–Neoproterozoic multi-rifting events in the North China Craton and their geological significance: a study advance and review. *Tectonophysics*, **662**, 153–166, https://doi.org/10.1016/j.tecto.2015.01.019

Zhang, K. and Shields, G.A. 2022. Sedimentary Ce anomalies: secular change and implications for paleoenvironmental evolution. *Earth-Science Reviews*, **229**, 104015, https://doi.org/10.1016/j.earscirev.2022.104015

Zhang, K. and Shields, G.A. 2023. Early diagenetic mobilization of rare earth elements and implications for the Ce anomaly as a redox proxy. *Chemical Geology*, **635**, 121619, https://doi.org/10.1016/j.chemgeo.2023.121619

Zhang, K., Zhu, X. and Yan, B. 2015. A refined dissolution method for rare earth element studies of bulk carbonate rocks. *Chemical Geology*, **412**, 82–91, https://doi.org/10.1016/j.chemgeo.2015.07.027

Zhang, S., Wang, X. *et al.* 2016. Sufficient oxygen for animal respiration 1,400 million years ago. *Proceedings of the National Academy of Sciences of the United States of America*, **113**, 1731–1736, https://doi.org/10.1073/pnas.1523449113

Zhang, K., Zhu, X., Wood, R.A., Shi, Y., Gao, Z. and Poulton, S.W. 2018. Oxygenation of the Mesoproterozoic ocean and the evolution of complex eukaryotes. *Nature Geoscience*, **11**, 345–350, https://doi.org/10.1038/s41561-018-0111-y

Zhang, K., Tarbuck, G. and Shields, G.A. 2024a. Refining the carbonate-associated iodine redox proxy with leaching experiments. *Chemical Geology*, **646**, 121896, https://doi.org/10.1016/j.chemgeo.2023.121896

Zhang, K., Shields, G.A., Zhou, Y., Strauss, H., Struck, U. and Jensen, S. 2024b. The basal Cambrian carbon isotope excursion revealed in the Central Iberian Zone, Spain. *Precambrian Research*, **411**, https://doi.org/10.1016/j.precamres.2024.107526

Zhou, X.Q., Li, N., Liang, G.S., Li, L., Tang, D.J. and Fu, X. 2009. Sedimentary significance of the autochthonous glauconite in stromatolitic limestones of the Mesoproterozoic Tieling Formation in Jixian, Tianjin, North China. *Geological Bulletin of China*, **28**, 985–990.

Zhu, S., Zhu, M. *et al.* 2016. Decimetre-scale multicellular eukaryotes from the 1.56-billion-year-old Gaoyuzhuang Formation in North China. *Nature Communications*, **7**, 11500, https://doi.org/10.1038/ncomms11500